Tellus (1991), *43A*, 49–63

Moderately stable flow over a three-dimensional hill A comparison of linear theory with laboratory measurements

By ROGER S. THOMPSON, *Atmospheric Research and Exposure Assessment Laboratory, US Environmental Protection Agency, Research Triangle Park, NC 27711, USA*, MICHAEL S. SHIPMAN, *NSI Technology Services Corporation, Research Triangle Park, NC 27709, USA* and JAMES W. ROTTMAN*, *Department of Marine, Earth and Atmospheric Sciences, North Carolina State University, Raleigh, NC 27695, USA*

(Manuscript received 12 January 1989; in final form 19 July 1990)

ABSTRACT

Several series of experiments were performed in a stratified towing tank to study the near-field flow of a linearly stratified fluid over an isolated three-dimensional hill. Streamlines were obtained in the laboratory using a stereographic method to determine the paths of plumes of dye released upstream of the hill. Velocities over the hill center were obtained by analysis of video recordings of dye plumes and with a propeller anemometer. The results of these experiments are compared with numerical solutions, computed using Fast Fourier Transforms, of the linearized equations of motion for an inviscid fluid. Numerical solutions were obtained using two different upper boundary conditions: one represents flow in a fluid of infinite depth and the other flow in a fluid of finite depth. Near the hill surface, the predicted streamline deflections were quite similar in both cases except for Froude numbers close to one in the lee of the hill. Good agreement with the measurements is found for Froude numbers (based on the hill height) greater than about 2.0. For Froude numbers greater than about 4.0, flow patterns were observed to differ only slightly from those for neutral flow.

1. Introduction

The interest in the flow of a stably-stratified atmosphere over mountains has a long history. Miles (1969) and Smith (1979) have presented excellent reviews of earlier theoretical advances. Much of the earlier work was directed toward understanding the far-field lee wave structure. More recent concerns about the transport of air pollutants released in complex terrain have prompted efforts toward examining the flow upstream and nearer the hill's surface.

Of particular interest in the present work are the paths of streamlines around an isolated hill. Hunt et al. (1979), among others, showed that the most important factor in determining the location and magnitude of the maximum ground-level concentration of pollutants released from a source upwind of a hill is the closeness of the plume's centerline to the hill's surface. Since in steady flows plume paths follow streamlines, Hunt (1985) proposed incorporating the knowledge of streamline paths into a Gaussian plume model as a method of predicting ground-level concentrations. Since streamlines are strongly affected by the hill shape and by the stratification, it is essential for such a model to have an accurate method of predicting streamline paths for different hill shapes and stratifications.

Computational methods that use the fully nonlinear equations describing fluid motion over an arbitrarily shaped, isolated, three-dimensional hill are too complicated and time consuming to be used for computing streamline paths in a practical prediction method such as that described in

* Present address: Universities Space Research Association, NASA/Goddard Space Flight Center, Greenbelt, MD 20771, U.S.A.

the previous paragraph. Therefore, approximate methods must be used. The most common approximations are to assume that the fluid is inviscid and Boussinesq and that the streamlines are only slightly deflected by the presence of the hill, so that a linearized form of the governing equations accurately describes the motion. Several efficient numerical techniques for solving these approximate equations are currently available. Smith (1980) formulated a numerical method based on the Fast Fourier Transform that efficiently solves the inviscid linearized equations when the upstream flow is uniform and has a linear density gradient. Blumen and McGregor (1976) describe a numerical eigenfunction method that allows for shear in the upstream flow.

The main objectives of the present work are to produce a useful data set of real streamline paths over an isolated, three-dimensional hill with which approximate flow models can be compared and to examine how accurately the small-amplitude inviscid theory approximates this data set. To accomplish these, laboratory measurements were made of the flow field around a particular hill towed through a stably stratified water channel. Specifically, the streamlines near the hill surface were measured in the laboratory by using a stereographic technique for accurately locating the position of dye plumes from sources upstream of the hill. In addition, the velocity profile above the center of the hill was measured using video techniques as well as a propeller anemometer. The laboratory measurements were then compared with the results of numerical solutions of the linearized inviscid equations. The numerical techniques used were similar to those described by Smith (1980).

Since our laboratory experiments were performed in a towing tank, we extended Smith's (1980) solution to the case of a fluid of finite depth. That is, the linearized equations were solved with an upper boundary condition of no displacement at a finite height above the surface as well as with the traditional radiation condition.

The only previous measurements of streamline paths in stably stratified flow over three-dimensional topography apparently are those of Riley et al. (1976), and their measurements were restricted to extremely stable flows in which the streamlines travel around the hill in nearly horizontal planes. Baines (1979) made some observations of upstream blocking of stratified flow by three-dimensional obstacles in a towing tank but did not measure streamlines. Some preliminary reports on the work described in the present paper are given in Snyder et al. (1986) and Thompson and Shipman (1987).

The model hill used in the present study is an axisymmetric idealization of a real hill in Idaho called Cinder Cone Butte. This particular idealized hill has been used in many previous laboratory studies of plume dispersion and the real hill has been the subject of an extensive field study. Descriptions of the laboratory and field studies are contained in Lavery et al. (1982) and Strimaitis et al. (1983).

The paper is organized as follows. In Section 2 a brief outline of the linearized mathematical model is given. The experimental apparatus and procedures are described in Section 3. The experimental results are presented and compared with the theory in Section 4, and finally a summary of the results and some conclusions are given in Section 5. The pertinent details of the numerical method for solving the linearized model are outlined in the Appendix.

2. Theory

Consider the steady flow of an unbounded stratified fluid over an isolated hill as sketched in Fig. 1. The hill is located at the origin of a Cartesian coordinate system with coordinates x along the mean horizontal flow direction, y across the mean flow direction, and z upwards. In this coordinate system, the hill surface is specified by the equation $z = h(x, y)$. Upstream of the hill the flow has a uniform approach velocity U and is linearly stratified. Two upper boundary conditions will be considered. For an unbounded layer of fluid, a radiation condition is applied which is expected to yield results applicable to atmospheric flows. For a finite fluid depth, the vertical displacement at the

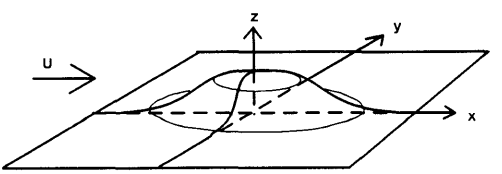

Fig. 1. Sketch of flow and coordinate system.

upper boundary is set to zero which models the experiments in the towing tank. Under the assumptions of small deflections, an inviscid, incompressible and nondiffusive fluid, the Boussinesq approximation, and negligible Coriolis forces, the equations representing the conservation of mass and momentum may be approximated as:

$$\frac{\partial u}{\partial x}+\frac{\partial v}{\partial y}+\frac{\partial w}{\partial z}=0 \tag{1}$$

$$U\frac{\partial \bar{\rho}}{\partial x}+w\frac{\mathrm{d}\bar{\rho}}{\mathrm{d}z}=0, \tag{3}$$

$$\rho_0 U\frac{\partial u}{\partial x}=-\frac{\partial p}{\partial x}, \tag{3}$$

$$\rho_0 U\frac{\partial v}{\partial x}=-\frac{\partial p}{\partial y}, \tag{4}$$

$$\rho_0 U\frac{\partial w}{\partial x}=-\frac{\partial p}{\partial z}-g\rho, \tag{5}$$

where u, v, and w are the velocity perturbations from the approach flow, ρ_0 is a reference density, ρ is the perturbation from the upstream density distribution $\bar{\rho}(z)$, which is assumed to be a linearly decreasing function of z, p is the perturbation of the pressure from its hydrostatic value, and g is the acceleration due to gravity. These are the linearized equations of motion.

It is convenient to express these equations in terms of a vertical displacement function. If the coordinates of a *fluid particle* moving through this steady flow field are represented as $[X(t), Y(t), Z(t)]$, where t is time, then a vertical displacement function $\eta(x, y, z)$ may be defined such that the vertical displacement of this particle from its far upstream height z_0 is given by $\eta(X, Y, Z)=Z-z_0$. In an analogous manner a lateral displacement function $\delta(x, y, z)$ may be defined such that $\delta(X, Y, Z)=Y-y_0$, where y_0 is the value of Y far upstream.

Within the approximations already made,

$$w=\frac{\mathrm{d}Z}{\mathrm{d}t}\simeq U\frac{\partial \eta}{\partial x}. \tag{6}$$

With this relationship (1)–(5) can be reduced to the following single equation for $\eta(x, y, z)$,

$$\frac{\partial^2}{\partial x^2}(\nabla^2\eta)+\frac{N^2}{U^2}\nabla_{\mathrm{H}}^2\eta=0, \tag{7}$$

where

$$\nabla_{\mathrm{H}}^2=\frac{\partial^2}{\partial x^2}+\frac{\partial^2}{\partial y^2}$$

and

$$N=\left(-\frac{g}{\rho_0}\frac{\mathrm{d}\bar{\rho}}{\mathrm{d}z}\right)^{1/2}$$

is the constant buoyancy frequency.

Application of the two-dimensional Fourier Transform pair (with the transform denoted by "$\hat{\ }$") defined by

$$\hat{\eta}(k, l, z)=\frac{1}{4\pi^2}\int_{-\infty}^{\infty}\int_{-\infty}^{\infty}\eta(x, y, z)\,\mathrm{e}^{-i(kx+ly)}\,\mathrm{d}x\,\mathrm{d}y, \tag{8}$$

and

$$\eta(x, y, z)=\int_{-\infty}^{\infty}\int_{-\infty}^{\infty}\hat{\eta}(k, l, z)\,\mathrm{e}^{i(kx+ly)}\,\mathrm{d}k\,\mathrm{d}l, \tag{9}$$

where k and l are the wavenumbers in the x and y directions, respectively, reduces (7) to

$$\frac{\partial^2\hat{\eta}}{\partial z^2}+m^2\hat{\eta}=0, \tag{10}$$

where

$$m^2=(k^2+l^2)(N^2/U^2-k^2)^2/k^2. \tag{11}$$

For an infinitely deep fluid, the solution of (10) is

$$\hat{\eta}(k, l, z)=\hat{\eta}(k, l, 0)\exp(imz) \tag{12a}$$

in which m is taken as the positive imaginary root of (11) if $k^2>N^2/U^2$ or the sign of m is the same as the sign of k if $k^2<N^2/U^2$ in order to eliminate an unbounded solution and to satisfy the radiation condition (i.e., energy may propagate only away from the hill). Now $\hat{\eta}(k, l, 0)$ can be found by transforming the linear boundary condition $\eta(x, y, 0)=h(x, y)$ to give

$$\hat{\eta}(k, l, 0)=\hat{h}(k, l). \tag{12b}$$

Thus, $\eta(x, y, z)$ can be expressed as

$$\eta(x, y, z)=\int_{-\infty}^{\infty}\int_{-\infty}^{\infty}\hat{h}(k, l)\,\mathrm{e}^{im(k,l)z}\mathrm{e}^{i(kx+ly)}\,\mathrm{d}k\,\mathrm{d}l. \tag{13}$$

With the transform of the hill shape specified or computed numerically, the double integral in (13) can be approximated numerically using Fast Fourier Transform techniques to produce the vertical displacement function.

The transforms of the perturbation velocity components can be found in terms of $\hat{\eta}$ as

$$\frac{\hat{u}(k, l, z)}{U} = \frac{-i}{m}\left(\frac{N^2}{U^2} - k^2\right)\hat{\eta}(k, l, z), \tag{14}$$

$$\frac{\hat{v}(k, l, z)}{U} = \frac{-il}{km}\left(\frac{N^2}{U^2} - k^2\right)\hat{\eta}(k, l, z), \tag{15}$$

$$\frac{\hat{w}(k, l, z)}{U} = ik\hat{\eta}(k, l, z). \tag{16}$$

In the linear approximation,

$$v = \frac{\mathrm{d}Y}{\mathrm{d}t} \simeq U\frac{\partial \delta}{\partial x} \tag{17}$$

and the transform of δ can be obtained from (15) in terms of $\hat{\eta}$ as

$$\hat{\delta}(k, l, z) = -\frac{l}{km^2}\left(\frac{N^2}{U^2} - k^2\right)\hat{\eta}(k, l, z). \tag{18}$$

Thus, with $\hat{\eta}$ given by (12), u, v, w and δ can be approximated by inverting (14), (15), (16) and (18) using Fast Fourier Transforms.

For a fluid layer of finite depth D, the upper boundary condition is $\eta(x, y, D) = 0$ which can be transformed to $\hat{\eta}(k, l, D) = 0$. With this boundary condition, the solution of (10) is

$$\hat{\eta}(k, l, z) = -\hat{h}(k, l)\sin(m(z - D))/\sin(mD), \tag{19}$$

in which m is taken as the positive root of (11).

Singularities (simple poles) exist at points in (k, l) space where $mD = n\pi$, for any integer n. For a fixed l, these singularities are located at $k = k_n(l)$, where

$$k_n^2(l) = \tfrac{1}{2}(N^2/U^2 - n^2\pi^2/D^2 - l^2) \pm \tfrac{1}{2}[(N^2/U^2 - n^2\pi^2/D^2 - l^2)^2 + 4N^2l^2/U^2]. \tag{20}$$

The real values of k_n are obtained by chosing the plus sign when $l \neq 0$ for $n = 1, 2, \ldots$. When $l = 0$, the singularities are on the real k axis at

$$k_n(0) = N^2/U^2 - n^2\pi^2/D^2, \qquad n = 1, 2, \ldots, n_k, \tag{21}$$

where n_k is an integer such that

$$n_k\pi < N/U < (n_k + 1)\pi. \tag{22}$$

These singularities must be considered in evaluating the inverse transform

$$\eta(x, y, z) = \int_{-\infty}^{\infty}\int_{-\infty}^{\infty} [-h(k, l) \times \sin(m(z - D))/\sin(mD)] \times \mathrm{e}^{i(kx + ly)}\,\mathrm{d}k\,\mathrm{d}l. \tag{23}$$

One method of evaluating (23) is to divide the part of the integrand in brackets into its analytic and principal parts and deal with each separately. The principal part can be obtained as

$$\hat{\eta}_P(k, l, z) = \sum_{n=1}^{n_l}\left(\frac{r_n^+}{k - k_n} + \frac{r_n^-}{k + k_n}\right),$$

$$n_l = \begin{cases} n_k, & \text{if } l = 0 \\ \infty, & \text{if } l \neq 0 \end{cases}, \tag{24}$$

where

$$r_n^{\pm} = \pm(n\pi/D^2)[N^2l^2/U^2k_n^2 + 1]^{-1} \times \sin(n\pi z/D)\,\hat{h}(k_n, l)/k_n \tag{25}$$

are the residues of $\hat{\eta}(k, l, z)$ at the poles located at $k = \pm k_n$. The analytic part is found by subtracting $\hat{\eta}_A = \hat{\eta} - \hat{\eta}_P$.

The inverse transform of the analytic part is obtained numerically with Fast Fourier Transforms as above. The principal part can be inverted by first considering the inner integral (with respect to k) which gives

$$\int_{\infty}^{\infty}\hat{\eta}_P(k, l, z)\,\mathrm{e}^{i(kx + ly)}\,\mathrm{d}k = \sum(r_n^+\,\mathrm{e}^{k_nx} + r_n^-\,\mathrm{e}^{-k_nx}). \tag{26}$$

Then, application of the numerical Fast Fourier Transform to (26) with respect to l will give $\eta_P(x, y, z)$. Application of Cauchy's Residue Theorem to the inner integral of (23) and the use

of group velocity concepts show that the contribution of these singularities are lee waves and apply only for $x>0$. Therefore, $\eta_P(x, y, z)$ for $x>0$ is added to the contribution from the analytic part.

Equations for the transforms of the lateral deflections and the velocity perturbations are derivable from the equations of motion and are similar in form to (19). They possess the same singularities which must be handled in the same manner.

The idealized circular hill shape studied here is represented by

$$h(x, y)=H/[1+(r/L)^4], \tag{27}$$

where $r^2=(x^2+y^2)$, H is the hill height and L is a lateral scale of the hill. An approximate sketch of this hill is shown in Fig. 1. The transform of this hill shape is

$$\hat{h}(k, l)=-\frac{1}{2\pi}HL^2\,\mathrm{kei}(\kappa L) \tag{28}$$

where $\kappa=(k^2+l^2)^{1/2}$ and kei is a Kelvin function, as defined by Abramowitz and Stegun (1964). For comparison, the transform of Crapper's hill shape

$$h(x, y)=H/[1+(r/L)^2]^{3/2}, \tag{29}$$

which was used in the theoretical studies of Crapper (1959) and Smith (1980) is

$$\hat{h}(k, l)=\frac{1}{2\pi}HL^2\exp(-\kappa L). \tag{30}$$

Both of these transformed hill spaces are plotted in Fig. 2. (Also plotted is the transform of a truncated version of (27) that will be described in the next section. For the purpose of comparison, the plots in Fig. 2 have been scaled so that the three hills have the same mean radius.)

The two nondimensional parameters in the infinite-depth problem are $F=U/(NH)$, which we define as the Froude number of the flow, and $A=H/L$, the aspect ratio of the hill. The assumption that the hill generates small amplitude disturbances requires F to be large and A to be small. Just how large F and how small A have to be to give a reasonably accurate approximation

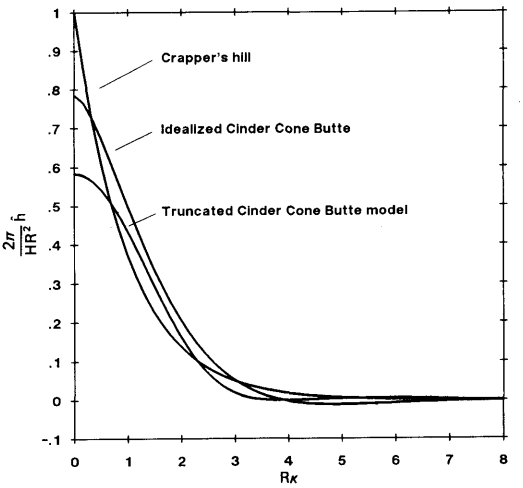

Fig. 2. Fourier Transform of hill shapes. (R is the mean radius of the hill; for Crapper hill, $R=L$; for idealized CCB, $R=1.111L$; for truncated CCB, $R=1.012L$)

to the fully nonlinear flow is difficult to determine from analysis alone. Generally, for a specified value of A, a critical value of F, say F_c, can be estimated at which the linear theory produces a vertical streamline, implying the onset of wave breaking somewhere in the flow. Since wave breaking means that nonlinear effects are important, the linear approximation would be expected to be accurate only when $F>F_c$. A typical value of $F_c\approx 2.0$ was computed by Smith (1980) for hydrostatic flow over Crapper's hill.

In the finite-depth problem, an additional parameter is H/D. The linearized approximation also requires this parameter to be small.

In practice, it appears that at least $A<1.0$ and $H/D<1.0$ are required for the linear theory to produce a reasonably accurate approximation near the hill surface. The hill used in the experiments described in the next section has $A\approx 0.4$ and $H/D\approx 0.14$. This value of A is quite large for valid use of linear approximations and perhaps a nonlinear analysis would be warranted.

Computer programs using Fast Fourier Transforms were written to approximate the Fourier Transform of a specified hill of arbitrary shape and the inverse Fourier Transforms of (13), (14), (15), (16) and (18) were found for an infinite-depth fluid. The numerical methods are outlined in the

Appendix. Similar techniques were used for the finite-depth fluid which dealt with the singularities as discussed above.

3. Experimental details

The experiments were performed in the large stratified towing tank at the EPA Fluid Modeling Facility located in Research Triangle Park, North Carolina. The tank is 1.2 m deep, 2.4 m wide and 25 m long. The test section of this tank has clear acrylic plastic walls and floor to provide maximum visual access. Salt water with salt concentration varying in the vertical was used to produce the stratification. In most of the experiments described here, the density profiles were linear with a buoyancy frequency, $N = 1.33$ rad s^{-1}. The specific gravity of the salt water varied from 1.2 at the bottom of the tank to 1.0 at the free surface. The depth of the fluid was typically 109 cm which is about 7 times the height of the model hill. A detailed description of the towing tank and its operating procedures is given in Thompson and Snyder (1976) and Hunt and Snyder (1980).

A towing carriage that travels on rails mounted on the sidewalls of the tank allowed model obstacles to be towed along the length of the tank at speeds that can be varied between 2 cm s^{-1} and 50 cm s^{-1}. The hill was mounted on a flat baseplate and this whole apparatus was suspended upside down from the carriage and towed at the surface of the water with the baseplate immersed about 0.5 cm. Although the model was towed in an inverted position the experiments will be discussed as though the model was in an upright position. The Froude number was varied in most cases by changing the tow speed U, although in a few cases the density gradient was decreased.

The model used in the experiments was a truncated version of (27) given by

$$h(r) = \begin{cases} (H+c)/[1+(r/L)^4] - c, & r \leqslant 5H \\ 0, & r > 5H \end{cases}, \tag{31}$$

with $H = 15.45$ cm, $L = 38.75$ cm, and $c = 0.97$ cm. As shown in the figures, the model had a fairly flat top and a maximum slope of 0.45 or 24.4°. The model was truncated so that when mounted on the towing-tank baseplate it blended smoothly into the flat surface at a radius of $5H$. Reference circles were painted on the model at various elevations to aid in the flow visualization. The numerical transform of this truncated hill is plotted in Fig. 2.

Fig. 3 shows the arrangement of the model and still cameras about the tank. The tracer used in these experiments was a blue food dye diluted with sufficient salt water to produce a plume that was neutrally buoyant at the release height. This mixture was released from a bent-over stack located near the upstream edge of the baseplate ($x = -7.5H$). For these experiments, a narrow plume was desired, so that a thin tube (1.5 mm ID) was used for the stack and the dye mixture was emitted nearly isokinetically to form a streamtube. For most of the tows, two or three stacks were used.

The technique developed to measure the three-dimensional plume trajectories is an application of the common stereographic process in which two simultaneous photographs taken from different vantage points are combinded to provide a three-dimensional representation. Both side- and bottom-view cameras moved with the model as it was towed so that several photos were obtained during each tow. The side-view camera was suspended from the towing carriage and directed obliquely upwards through the layers of salt water to avoid internal reflections. The bottom-view camera was

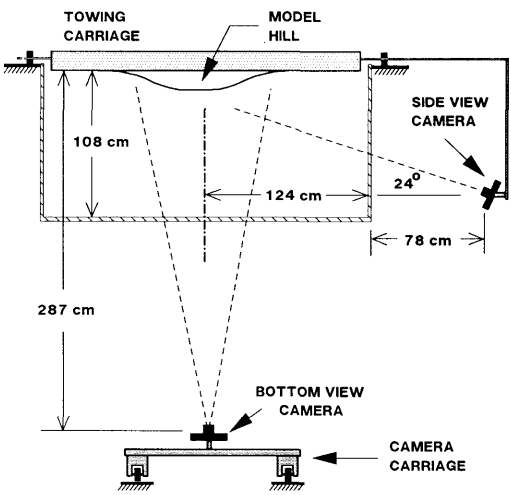

Fig. 3. Cross section of towing tank showing model and camera arrangement.

mounted on a second carriage below the tank that moved synchronously with the model. The cameras were triggered simultaneously by radio command.

The rather tedious process of resolving the three-dimensional trajectory from pairs of photographs is described in detail by Snyder et al. (1986). Parallax and refraction of the light through the stratified fluid were considered in computing the true positions from the photographic representations. Each measured streamline was obtained by averaging three realizations. The error analysis shows that plume trajectories were measured to within 1 cm of their true positions.

Vertical profiles of velocity were obtained over the center of the hill for a range of Froude numbers using another photographic technique. A video camera was mounted on a rigid support extended from the towing carriage to provide a side view of the central part of the hill and the area above it. Also included in the field of view were vertical rods of known height and separation as references for determining the positions of dye markers as they passed over the hilltop.

The video recording of the dye as it passed over the hilltop was played back on a stop-action recorder/monitor system that was connected to a "frame grabber" board in a personal computer. The recording was scanned by eye to find a segment of a dye plume that contained a characteristic feature (marker) that moved through the field of view. The video image was digitized. The position of the marker was determined and then tracked through successive frames on the video tape. The marker's speed was obtained by determining the distance the marker traveled (typically about 20 cm) through a number of video frames. The estimated maximum error in determining the velocity is about 8%.

Additional measurements of the average speed over the hill center were made with a propeller anemometer (Enercorp Instruments Ltd., Mikromini - water I, model 642w - m/1). The diameter of the propeller blade was 0.8 cm. This unit was installed on the end of a boom that extended from the rear of the towing carriage so that the propeller was positioned directly below the center of the inverted hill with the boom off to one side. The indicated speed on the instrument's meter was observed over the duration of each tow and averaged by eye. Repeated calibrations indicated that the propeller anemometer measured speeds to within a maximum error of about 10%. Measurements were made for Froude numbers of 1.0, 1.5, 2.0 and neutral flow at heights above the hill center of $(z-H)/H = 0.25$ and 1.0.

4. Results

Streamline trajectories were measured for Froude numbers of $F = 1.0$, 2.0, 3.0, 4.0, 6.0, 8.0, and ∞ (neutral flow). Sideview photographs of dye plumes originating on the centerline far upstream are shown in Fig. 4 and planview photographs of dye plumes originating off the centerline are shown in Fig. 5 for Froude numbers 1.0, 2.0 and ∞. These photographs show the basic qualitative features of the near field flow as a function of Froude number.

The sideview photographs show that at $F = 1.0$ and 2.0 the flows exhibit large downward vertical deflections over the lee side of the hill. These were observed to persist far downstream. In contrast, at $F = \infty$, the flow has a more nearly symmetric streamline pattern over the upstream and downstream sides of the hill. The planview

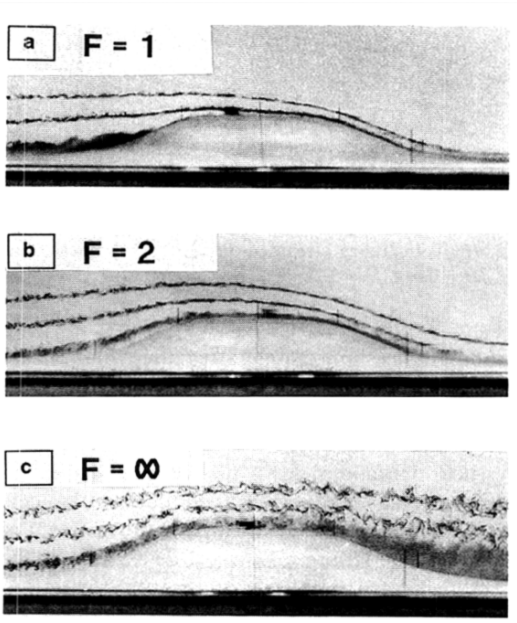

Fig. 4. Side view of centerline dye plumes released at $z_0/H = 0.25$, 0.75, and 1.25. Flow is left to right.

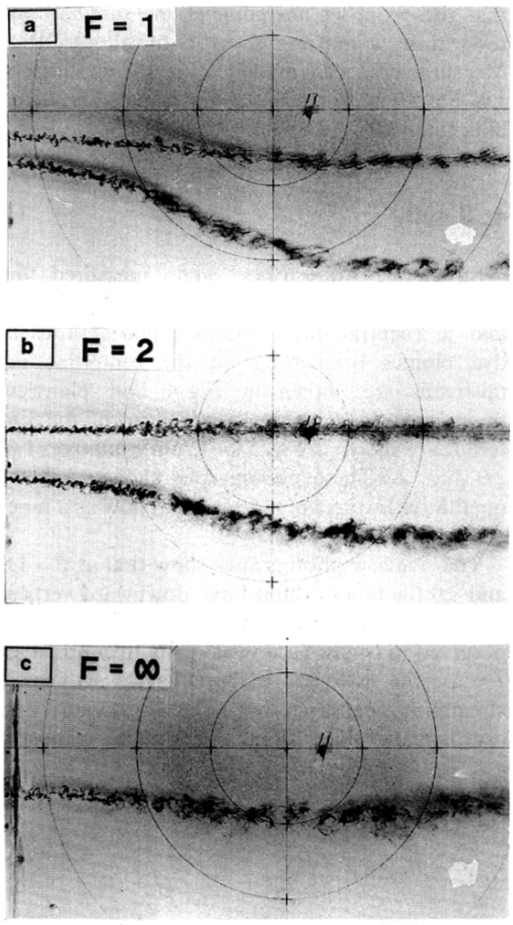

Fig. 5. Overhead view of dye plumes released at $y_0/H = -1.0$, $z_0/H = 0.25$. Flow is left to right. Extra streamer on top in (a) released at $y_0/H = -0.5$, $z_0/H = 0.75$. Extra streamer on top in (b) released at $y_0/H = 0.0$, $z_0/H = 0.5$.

photographs show that the streamlines in the flows at $F = 1.0$ and 2.0 have lateral deflections that persist for large distances downstream of the hill. This horizontal divergence is associated with the large vertical deflections down the lee side of the hill. Again, in neutral flow the streamlines in planview are fairly symmetric upstream and downstream of the hill. The strong downward deflections in the stratified cases completely suppress the separation on the lee side of the hill that appears in the neutral case. Another feature of the flow to note is that the dye plumes are much more diffuse in neutrally stratified flow than in stratified flow. This feature is most evident in the sideview photographs; turbulent diffusion, particularly in the vertical, is suppressed by stratification.

Quantitative measurements of dye plume trajectories originating on the centerplane, far upstream, at heights of $z_0/H = 0.25$, 0.50, 0.75, 1.00, 1.25, and 1.50 were determined for all Froude numbers for which experiments were performed. Also, the trajectories originating at laterally offset positions of $(y_0/H, z_0/H) = (2.0, 0.50)$ and $(2.5, 0.25)$ were obtained for all Froude numbers. In addition, trajectories for some other laterally offset position were obtained for some Froude numbers. Only small differences were observed in the flow patterns for Froude numbers at or above 6.0. That is, for $F = 6.0$ and 8.0 the flow field was essentially the same as for neutral flow. This was also found to be true in the numerical calculations.

Fig. 6 shows the comparison of the measured and computed streamlines on the centerplane over the hilltop for different Froude numbers. Results from computions using both upper boundary conditions, infinite fluid depth and finite fluid depth (with $D/H = 7.0$), are presented as two styles of dashed lines. As anticipated, comparisons for the $F = 1.0$ case (Fig. 6a) were not good. In fact, some of the computed streamlines intersect the hill surface. The measured streamlines exhibit a strong convergence over the hilltop and closely approach the hill surface on the lee side. The dye plume originating at a height of $z_0/H = 0.25$ was tracked only to a point near the upstream surface of the hill where it probably impacts on the hill and then is spread broadly and thinly to cover the entire hill surface above the release level. The comparisons of measured and computed centerplane streamlines were better for $F = 2.0$, 3.0, 4.0, and ∞. At $F = 2.0$ the computed and measured streamlines compare very well upstream and over the top of the hill but not as well downstream where the measured streamlines have larger vertical deflections. In the lee of the hill at $F = 2.0$, the finite depth predictions are somewhat closer to the measurements than are those assuming an infinite depth of fluid. At $F = 3.0$, the streamlines are better predicted downstream but less well predicted over the top of the hill compared with the $F = 2.0$ case. These rough comparisons continue to hold true for $F > 3.0$.

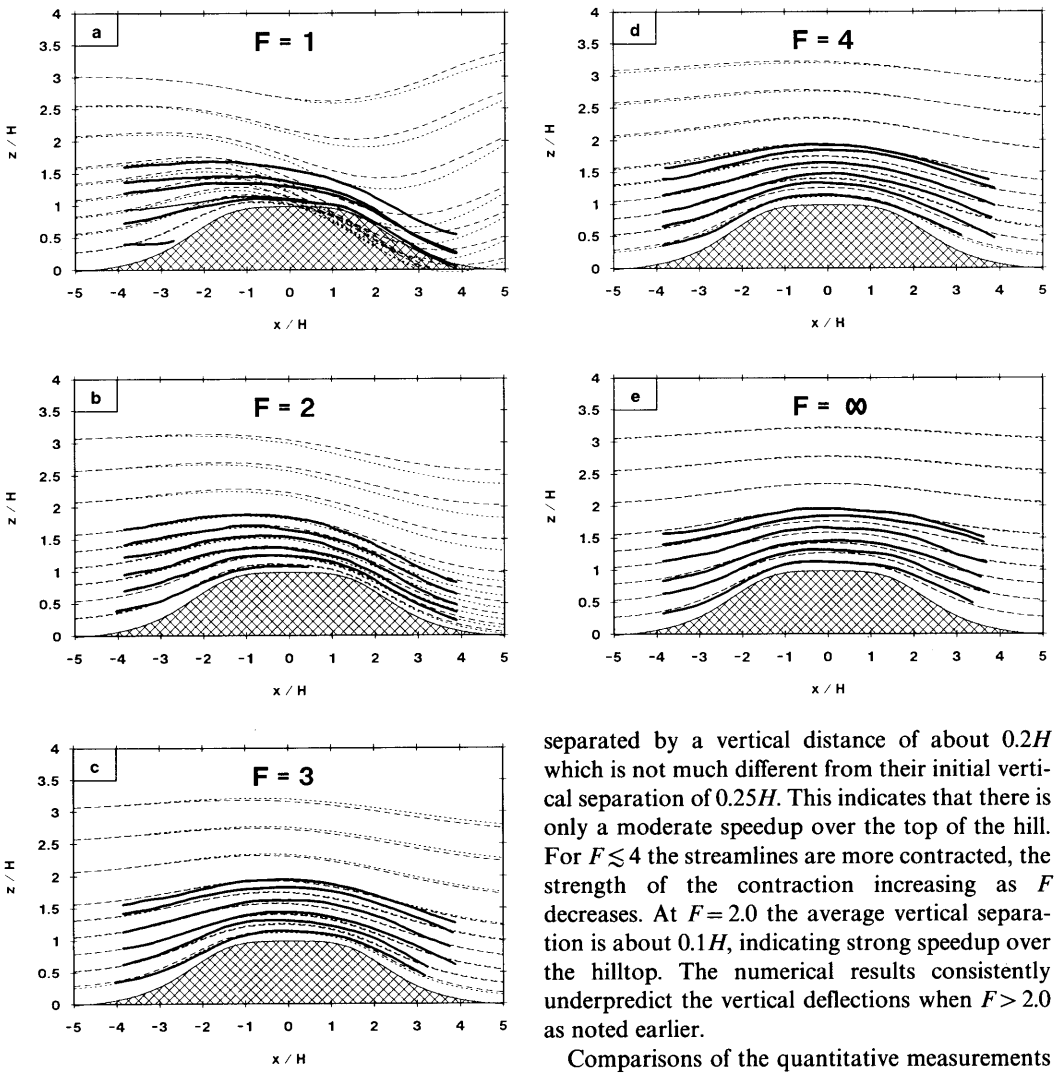

Fig. 6. Measured and calculated centerline streamlines over ACC. ----- Calculations - infinite depth, ------- Calculations - finite depth, ——— Towing-tank measurements.

The effects of stratification on vertical deflections of streamlines can be seen in Fig. 7, which shows the measured streamline heights above the top center of the hill as a function of Froude number for all 6 release heights. Again, the dashed lines in the plot show the numerical results. In this figure, it is seen that significant departures from neutral flow ($F=\infty$) occur for Froude numbers less than about 4.0. For $F \gtrsim 4$ the streamlines are separated by a vertical distance of about $0.2H$ which is not much different from their initial vertical separation of $0.25H$. This indicates that there is only a moderate speedup over the top of the hill. For $F \lesssim 4$ the streamlines are more contracted, the strength of the contraction increasing as F decreases. At $F=2.0$ the average vertical separation is about $0.1H$, indicating strong speedup over the hilltop. The numerical results consistently underpredict the vertical deflections when $F>2.0$ as noted earlier.

Comparisons of the quantitative measurements of the lateral deflections with the computed results for streamlines originating at a height of $z_0/H=0.25$ at several values of y_0/H for Froude numbers 1.0, 2.0 and ∞ are shown in Fig. 8. The difference between predicted lateral deflection for finite and infinite depths of fluid are small for all cases. The computed trajectories do not match the measured ones very well for Froude numbers 1.0 and 2.0, although the agreement is quite good at $F=\infty$. Lateral deflections for streamlines originating at $z_0/H=0.5$ and 1.0 are shown in Figs. 9 and 10. Note that in some cases, two realizations of a measured trajectory are plotted (e.g., Fig. 9b, for $y_0/H=2.0$ and Fig. 10c). The agreement

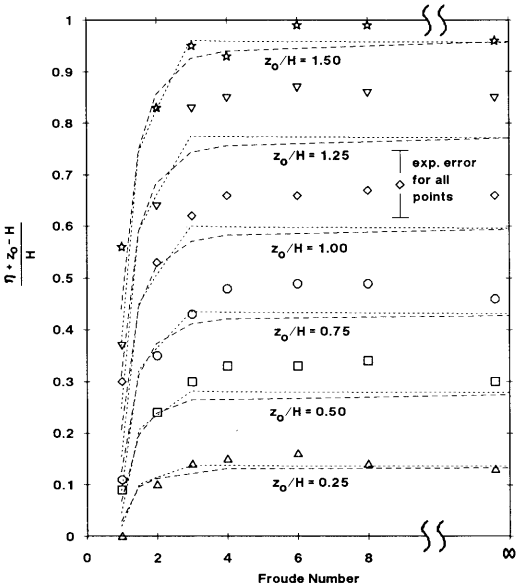

Fig. 7. Distance of streamlines above hilltop at center of hill for various release heights. ——— Calculations - infinite depth, ------- Calculations - finite depth. Measured values: Δ, $z_0/H = 0.25$; □, $z_0/H = 0.50$; ○, $z_0/H = 0.75$; ◇, $z_0/H = 1.00$; ▽, $z_0/H = 1.25$; and ☆, $z_0/H = 1.50$.

between measured and computed streamlines gets increasingly better as z_0/H increases. The measured streamlines tend to have larger lateral deflections than the computed streamlines in the presence of stratification; at $F = 1.0$ and $z_0/H = 0.25$, our worst case, the difference between the computed and measured lateral deflections are as much as $2H$. For neutral flow the measured trajectories meander more than in the stratified cases due to the experimental factors discussed above, but the mean trajectories compare quite well with the computations.

A distinct observation drawn from the plots of lateral deflections is that at the lower values of F the lateral deflections persist for a significant distance downstream. As shown by Smith (1980), the theory predicts that lateral deflections will persist farther downstream the closer z_0 is to 0 and at $z_0 = 0$ the lateral deflections are permanent.

Vertical profiles of the measured and computed streamwise component of velocity above the hill center are shown in Fig. 11 for $F = 1.0$, 1.5, 2.0 and ∞. The infinite depth values are slightly larger than those for finite depth. They do not match the measurements well at $F = 1.0$. For larger Froude numbers the calculations are reasonably good approximations to the data, although there is considerable scatter in the data at the lower Froude numbers. None of the experimental cases produced a strong localized jet above the hill; for this flat topped hill, there was a fairly deep layer of nearly

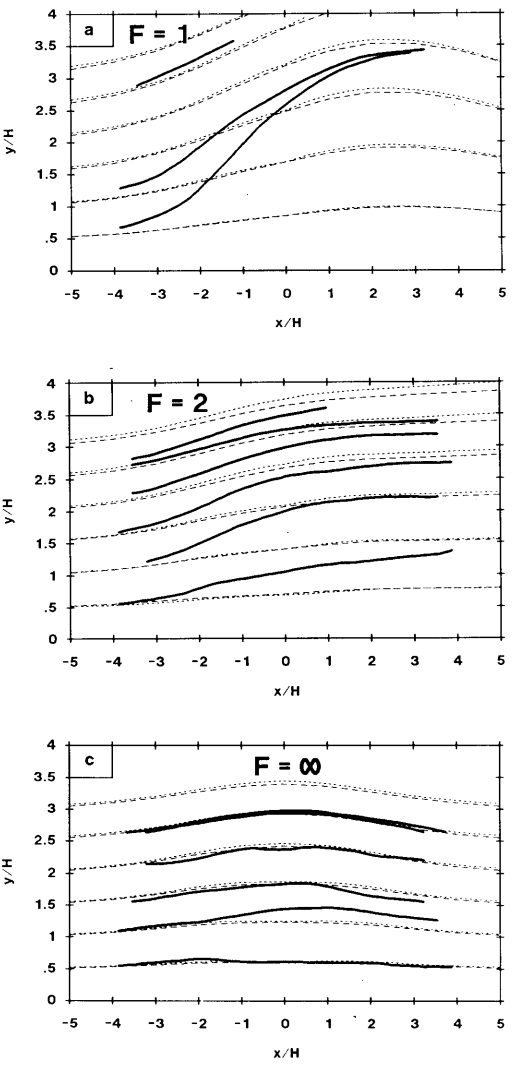

Fig. 8. Top view of streamlines originating at $z_0/H = 0.25$. ——— Calculations - infinite depth, ------- Calculations - finite depth, ——— Towing-tank measurements.

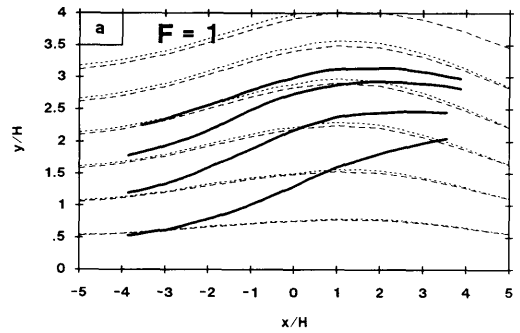

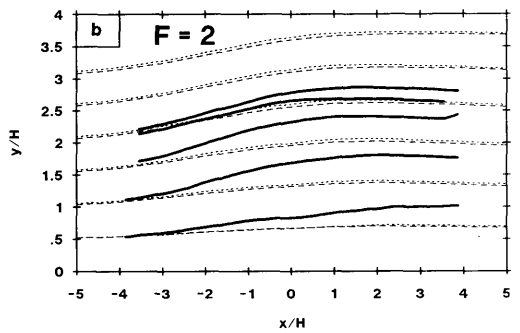

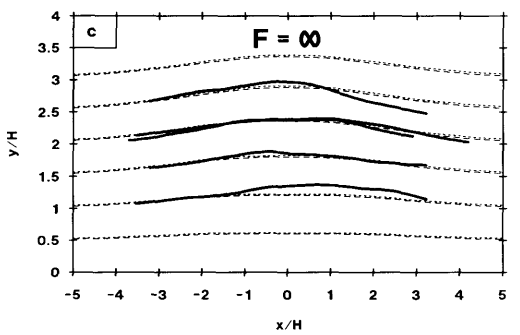

Fig. 9. Top view of streamlines originating at $z_0/H = 0.25$. ----- Calculations - infinite depth, ------- Calculations - finite depth, ——— Towing-tank measurements.

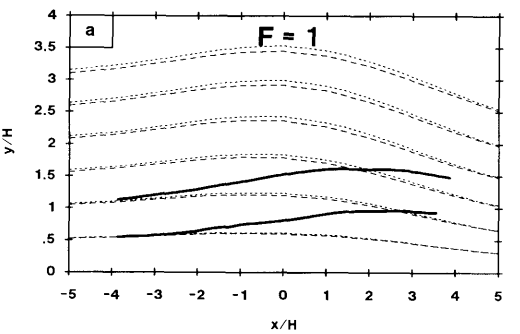

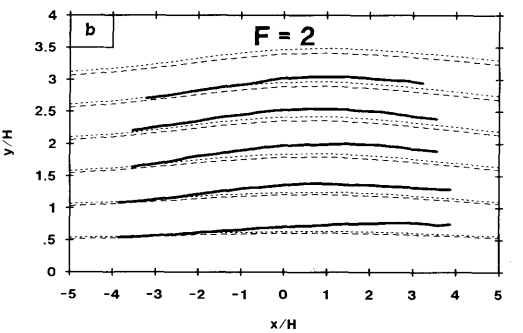

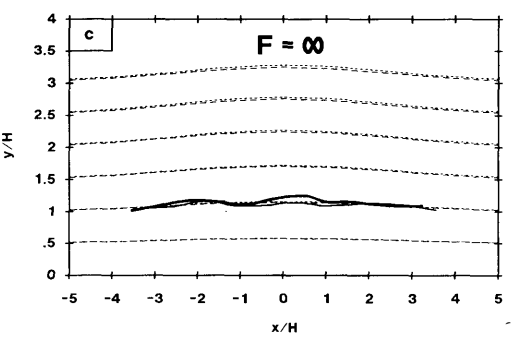

Fig. 10. Top view of streamlines originating at $z_0/H = 0.25$. ----- Calculations - infinite depth, ------- Calculations - finite depth, ——— Towing-tank measurements.

constant flow speedup. The measured speed of the flow showed a maximum increase over the uniform upstream speed of about 45% at $F = 1.0$ and increases of about 15% for $F = 2.0$ and neutral flow. The speed in the thin layer just above the top of the hill decreases as the Froude number decreases. A fluid particle traveling along the streamline that just passes over the top of the hill has to give up more of its kinetic energy to potential energy as the stratification increases, so that its speed at the hilltop will decrease as the Froude number decreases. On the other hand, the tendency for streamlines to pass around the hill as the Froude number decreases results in a smaller upward vertical deflection over the top of the hill, so the fluid speed at a small distance above the

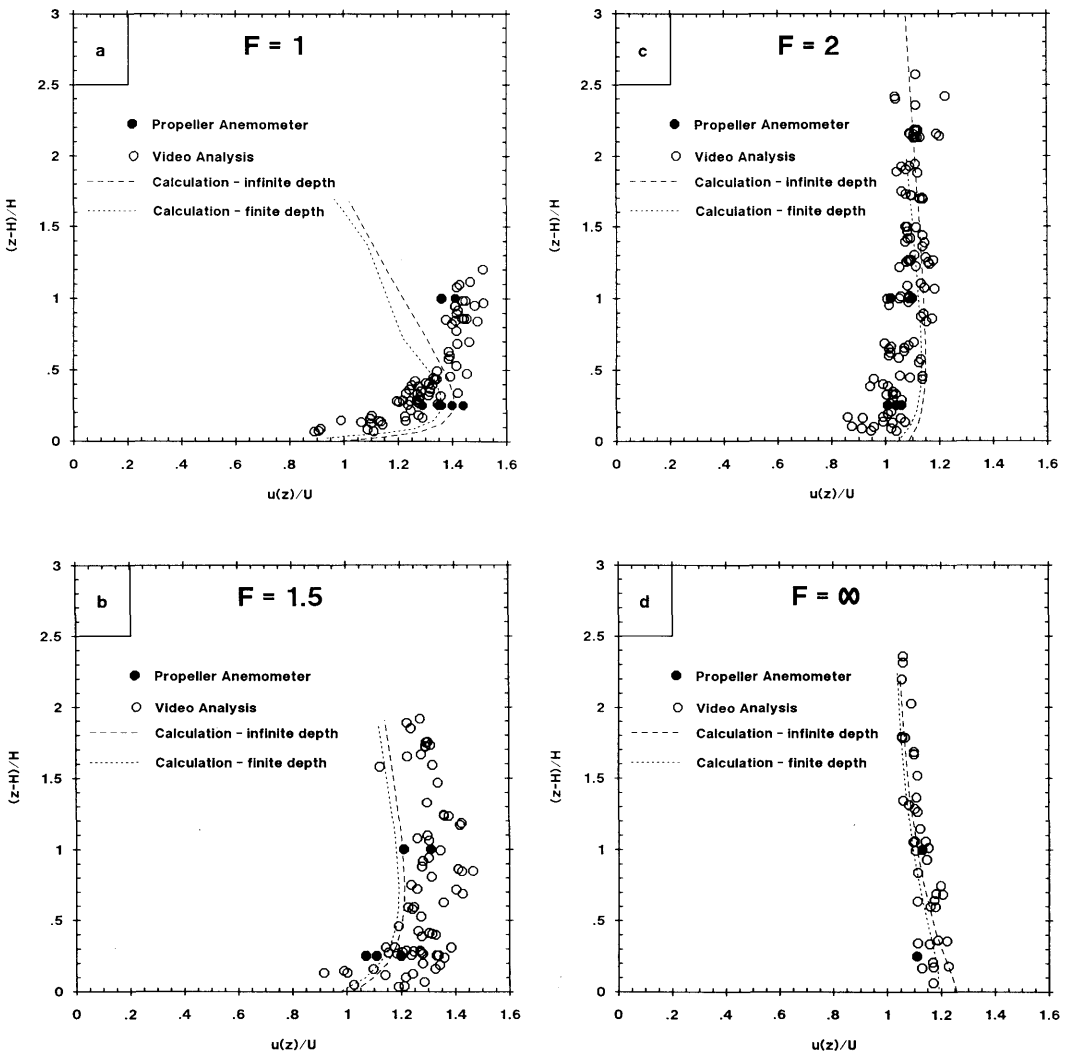

Fig. 11. Vertical profiles of downwind velocity component over hill center.

hilltop has to increase as the Froude number decreases. The combination of these two effects causes the small jet at the hilltop for Froude numbers less than about 2.0.

Another important feature of the real flow in the laboratory is separation on the lee side of the hill. This occurs in our experiments in neutrally stratified flow because the hill is rather steep. And because the Reynolds number is large the flow usually separates near the crest of the hill. In stably stratified flow, it is possible for the lee wave properties of the flow to suppress this separation. The experiments of Hunt and Snyder (1980) on stably stratified flow over three-dimensional hills provide some guidance on this point. They showed that lee side separation in stably stratified flows is determined by the parameter $\lambda/4L$, where $\lambda = 2\pi U/N$ is the fundamental lee wave wavelength and $4L$ is the appropriate streamwise length of the hill. When $\lambda/4L \gg 1$, the flow over the hill is like that of neutral flow; that is, separation is controlled by the pressure field in the boundary layer

over the ridge. For the present case, this means that the flow separates near the crest. When $\lambda/4L$ is of order 1, separation is determined by the pressure field associated with the lee waves. When $\lambda/4L \approx 1$, the lee wave closely matches the contour of the hill and separation is completely suppressed. When $\lambda/4L < 1$, separation occurs at the location of the trough of the first lee wave; that is, the separation point is located at $x_s \approx (1/2)\lambda$, where x_s is the value of x at the point of separation. For the particular hill used in this study, the above argument tells us to expect complete suppression of separation at Froude numbers of the order of unity. From observation, it appears that separation was suppressed for Froude numbers in the range 1.0 to 2.0.

5. Summary and conclusions

Streamlines were computed for both an infinitely deep fluid and one of finite depth (with $H/D = 0.14$, as for the towing tank). Near the hill, the streamlines obtained from the finite-depth calculations differed only slightly from those calculated assuming an infinite depth.

The computed streamline paths matched the measured ones quite well for Froude numbers greater than or equal to about 2.0. For the Froude number 1.0 case, the measured streamlines had smaller vertical deflections downstream of the hill and much larger lateral deflections than the computations. The differences between measured and computed trajectories were largest near the surface. At lower Froude numbers in the lee of the hill, the finite depth calculations gave somewhat better agreement with the measurements.

Vertical profiles of the streamwise component of velocity measured above the hilltop compared quite well with the computed values for Froude number greater than and about equal to 2.0. At Froude numbers of 1.5 and especially 1.0, the agreement was not as good. A fairly deep layer of maximum speedup was observed for all cases. The measured speed ratio over the approach flow for Froude number 1.0 was about 1.5 and for neutral flow was about 1.2.

The observed near-field flows did not differ significantly from neutral flow for Froude numbers as low as 6.0, and the differences were minor down to a Froude number of 4.0. For Froude numbers less than 4.0, the near field flow was markedly different from neutral flow.

The main conclusion of this work is that the numerical solution of the inviscid linearized equations for stratified flow over an isolated three-dimensional hill is an accurate method for predicting streamline paths in real flows for Froude numbers, based on the hill height, greater than or equal to about 2.0 even though $A \approx 0.4$. This lower limit of the Froude number for the accuracy of the linear approximation is consistent with the arguments presented by Smith (1980) for the critical Froude number at which a vertical streamline first appears in the flow. (The vertical streamline that should appear above the hill at $F = 2.0$ is not shown in Figs. 6 or 7 because it occurs at $z/H \approx 3\pi$, much higher than any dye plumes used in these experiments.)

The calculations performed in this analysis are first order in that they are based on linear approximations to the equations of motion. It was assumed that the perturbations of velocity and the streamline displacements were small so that higher order terms could be ignored. The calculations could be improved by using a nonlinear analysis. If second order terms were retained, solution would involve using the first order solutions to derive the second order equations which would be inhomogeneous. Solution of these would result in better calculation of the flow for smaller Froude numbers and larger aspect ratio hills where the assumptions of small perturbations are not strictly valid.

Another important feature lacking in the linear theory used in this paper is the ability to incorporate shear in the upstream flow. For the type of flows produced in a towing tank there is, of course, no shear in the upstream flow. But in real situations in the atmosphere or in a meteorological wind tunnel, the flow over a hill will be a boundary-layer type flow that is strongly sheared close to the ground. It is important to incorporate this effect into the prediction model. Perhaps a numerical method similar to that used by Blumen and McGregor (1976) could be used for such flows.

6. Acknowledgements

The support of the entire staff of the EPA Fluid Modeling Facility during this research effort is

appreciated. Special thanks are extended to William H. Snyder, G. Leonard Marsh, P. Scott Johnson, Paul Bookman, and Robert Lawson, Jr. We also acknowledge helpful discussions with D. A. Smeed at Cambridge University. JWR acknowledges financial support from the U.S. Environmental Protection Agency through the cooperative agreement CR-811973 with North Carolina State University.

Disclaimer. Although the research described in this article has been supported by the United States Environmental Protection Agency, it has not been subjected to Agency review and therefore does not necessarily reflect the views of the Agency and no official endorsement should be inferred. Mention of trade names or commercial products does not constitute endorsement or recommendation for use.

7. Appendix. Numerical methods

FORTRAN 77 programs, designed to run on an IBM PC-XT microcomputer, were written to evaluate the integrals described in Section 2. The main part of each program was the Fast Fourier Transform (FFT) subroutine. The particular routine used for the calculations described here is commercially available under the trade name 87FFT from MicroWay, Inc. of Kensington, MA. In what follows we will describe the procedure to obtain $\eta(x, y, z)$, since the method is essentially the same for the other dependent variables in the problem.

A two-dimensional rectangular grid is constructed over the $x-y$ plane of the computational domain with a constant mesh size Δx in the x direction and Δy in the y direction. The hill shape $h(x, y)$ on this grid is then transformed using the FFT routine to produce $\hat{h}(k, l)$ on a two-dimensional grid in $k-l$ space with grid spacing $\Delta k = 2\pi/(N_x \Delta x)$ and $\Delta l = 2\pi/(N_y \Delta y)$, where N_x and N_y are the number of grid points in the x and y directions, respectively.

One complication in performing the inverse transform of $\hat{\eta}(k, l)$ that was not dealt with in the text is the treatment when $k = 0$. These singular parts were subtracted from the integrands before numerical inversion, and the final solution was adjusted by adding a constant to make $\eta(x, y) \Rightarrow 0$ as $x \Rightarrow -\infty$.

Another difficulty with the use of the FFT technique is that it is a finite Fourier transform. This implies that the hill is repeated periodically in both the x and y directions. To avoid the influence of these other hills, the computational domain must be made large enough so any disturbance they create is negligibly small. On the other hand, the grid size in the computational domain must be small enough to fully resolve the hill. After several sample runs with different numbers of grid points and grid spacings, it was found that $N_x = N_y = 256$ and $\Delta x = \Delta y = H$ satisfied all the restrictions.

As a reference for the computation time, the calculations to determine $\eta(x, y, z_0)$ for the infinite-depth case at a specified value of z_0 required about an hour on an IBM PC-XT with its 8088 microprocessor and 8087 math coprocessor running at 4.77 MHz.

REFERENCES

Abramowitz, M. and Stegun, I. A. 1964. *Handbook of mathematical functions.* National Bureau of Standards Applied Mathematics Series 55, Wahington, D.C.

Baines, P. G. 1979. Observations of stratified flow past three-dimensional barriers. *J. Geophys. Res. 84, no. C12,* 7834–8.

Blumen, W. and McGregor, C. D. 1976. Wave drag by three-dimensional mountain lee-waves in nonplanar shear flow. *Tellus 28,* 287–298.

Crapper, G. D. 1959, A three-dimensional solution for waves in the lee of mountains. *J. Fluid Mech. 6,* 51–76.

Hunt, J. C. R. 1985. Turbulent diffusion from sources in complex flows. *Ann. Rev. Fluid Mech. 17,* 447–85.

Hunt, J. C. R., Puttock, J. S. and Snyder, W. H. 1979. Turbulent diffusion from a point source in stratified and neutral flows around a three-dimensional hill, part I: diffusion equation analysis. *Atmos. Envir. 13,* 1227–1239.

Hunt, J. C. R. and Snyder, W. H. 1980. Experiments on stably and neutrally stratified flow over a model three-dimensional hill. *J. Fluid Mech. 96,* 671–704.

Lavery, T. F., Bass, A., Strimaitis, D. G., Venkatram, A., Green, B. R., Drivas, P. J. and Egan, B. A. 1982. *EPA Complex terrain modeling program: first milestone report - 1981.* Rpt. No. EPA-600/3-82-036, Env. Prot. Agcy., Res. Tri. Pk., NC.

Miles, J. W. 1969. Waves and wave drag in stratified flows. Proc. 12th Int. Congress Applied Mechanics, (eds., M. Hetenyi and W. G. Vincenti.) Springer-Verlag, 52–76.

Riley, J. J., Liu, H. T. and Geller, E. W. 1976. *A numerical and experimental study of stably stratified flow around complex terrain.* Envir. Prot. Agcy., Rpt. No. EPA-600/4-76-021, Res. Tri. Pk. NC.

Smith, R. B. 1979. The influence of mountains on the atmosphere. *Adv. Geophys. 21*, 87–230.

Smith, R. B. 1980. Linear theory of stratified hydrostatic flow past an isolated mountain. *Tellus 32*, 348–64.

Snyder, W. H., Thompson, R. S., and Shipman, M. S. 1986. Streamline trajectories in neutral and stratified flow over a three-dimensional hill, Appendix, *EPA Complex Terrain Model Development Fifth Milestone Report - 1985*, Envir. Prot. Agcy., Rpt. No. EPA-600/3-85-069, Res. Tri. Pk. NC., Jan.

Strimaitis, D. G., Venkatram, A., Greene, B. R., Hanna, S., Heisler, S., Lavery, T. F., Bass, A. and Egan, B. A. 1983. *EPA Complex terrain modeling program: second milestone report - 1982*, Rpt. No. EPA-600/3-83-015, Env. Prot. Agcy., Res. Tri. Pk., NC.

Thompson, R. S. and Shipman, M. S. 1987. Streamlines in stratified flow over a three-dimensional hill. *Preprint Vol. AMS 5th Jt. Conf. Appl. Air Poll. Meteorology with APCA*, Nov., Chapel Hill, NC, Amer. Meteorol. Soc., Boston, MA.

Thompson, R. S. and Snyder, W. H. 1976. EPA Fluid modeling facility, *Proc. Conf. on Modeling and Simulation*, Rpt. No. EPA-600/0-76-016, Envir. Prot. Agcy., Wash. D.C., July.